

## **SUPPORTING INFORMATION**

**SYNTHESIS AND MULTISTATE CHARACTERIZATION OF  
*BIS*-FLAVYLIUM DICATIONS –  
SYMMETRIC RESORCINOL- AND PHLOROGLUCINOL-  
TYPE DERIVATIVES AS STOCHASTIC SYSTEMS**

**Nuno Basílio,<sup>[a]</sup> Tony Garnier,<sup>[b]</sup> João Avó,<sup>[a]</sup> Mathieu Danel,<sup>[b]</sup>  
Stefan Chassaing<sup>\*[b]</sup> and Fernando Pina<sup>\*[a]</sup>**

<sup>[a]</sup> LAQV, REQUIMTE, Departamento de Química, Faculdade de Ciências e Tecnologia, Universidade Nova de Lisboa, 2829-516 Caparica (PORTUGAL) – *fp@fct.unl.pt*

<sup>[b]</sup> ITAV, Université de Toulouse, CNRS, UPS, 1 place Pierre Potier, 31106 Toulouse Cedex 1 (FRANCE) – *stefan.chassaing@itav.fr*

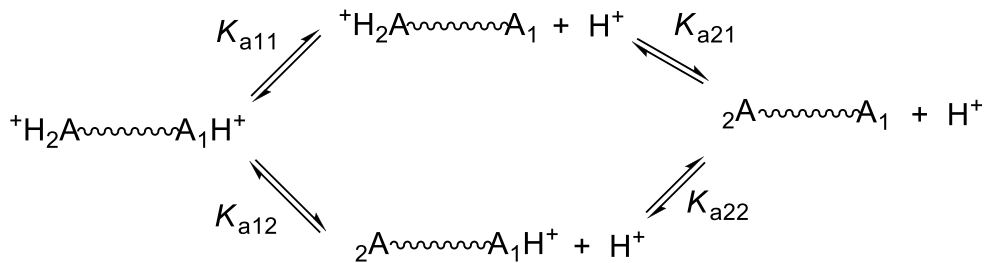
**Contents:**

<b>Appendix 1</b>	S1-S2
<b>Appendix 2</b>	S3-S4
<b>Compilation of NMR Spectra – <math>^1\text{H}</math>, <math>^{13}\text{C}</math> &amp; DEPT135</b>	S5-S16

---

## Appendix 1.

By considering two generic acidic groups  $\mathbf{A}_1\mathbf{H}^+$  and  $\mathbf{A}_2\mathbf{H}^+$  covalently connected by a spacer the following scheme can be proposed:



According to the above scheme four microscopic acid-base dissociation constants can be defined:

$$K_{a11} = \frac{[A_2H^+A_1][H^+]}{[A_2H^+A_1H^+]}$$

$$K_{a12} = \frac{[A_2A_1H^+][H^+]}{[A_2H^+A_1H^+]}$$

$$K_{a21} = \frac{[A_2A_1][H^+]}{[A_2H^+A_1]}$$

$$K_{a22} = \frac{[A_2A_1][H^+]}{[A_2A_1H^+]}$$

Defining an apparent acid-base dissociation constant for the formation of monocationic species:

$$K_{a1} = \frac{([A_2H^+A_1] + [A_2A_1H^+])[H^+]}{[A_2H^+A_1H^+]}$$

The concentration of monocationic species is given by:

$$[A_2H^+A_1] + [A_2A_1H^+] = \frac{K_{a11}[A_2H^+A_1H^+] + K_{a12}[A_2H^+A_1H^+]}{[H^+]}$$

So it can be demonstrated that the apparent  $K_{a1}$  is given by the sum of the microscopic

$$K_{a1} = \frac{\frac{K_{a1}[A_2H^+A_1H^+]}{[H^+]} - \frac{K_{a11}[A_2H^+A_1H^+] + K_{a12}[A_2H^+A_1H^+]}{[H^+]}}{K_{a1}} = K_{a11} + K_{a12}$$

Similarly for the formation of the neutral species:

$$K_{a2} = \frac{[A_2A_1][H^+]}{([A_2H^+A_1] + [A_2A_1H^+])}$$

$$[A_2H^+A_1] + [A_2A_1H^+] = \frac{[A_2A_1][H^+]}{K_{a21}} + \frac{[A_2A_1][H^+]}{K_{a22}}$$

$$[A_2H^+A_1] + [A_2A_1H^+] = \frac{[A_2A_1][H^+]K_{a22} + [A_2A_1][H^+]K_{a21}}{K_{a21}K_{a22}}$$

Combining the above expressions:

$$K_{a2} = \frac{K_{a21}K_{a22}}{K_{a22} + K_{a21}}$$

In stochastic systems, all microscopic constants are the same and equal to  $K_{am}$  and the following relationships can be found:

$$K_{a1} = K_{a11} + K_{a12} = 2K_{am}$$

$$K_{a2} = \frac{K_{a21}K_{a22}}{K_{a22} + K_{a21}} = \frac{K_{am}}{2}$$

$$\frac{K_{a1}}{K_{a2}} = 4$$

$$pK_{a2} = pK_{a1} + 0.6$$

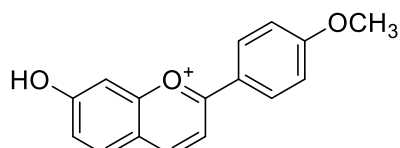
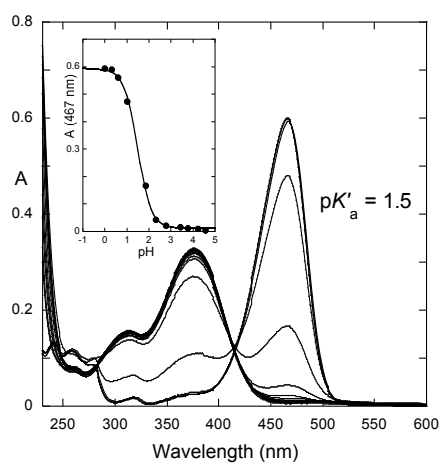


**Figure S1.** UV/Vis spectral variations occurring upon a direct pH jump from stock solutions of model compound 4'-methoxy-7-hydroxyflavylium to higher pH values at the thermodynamic equilibrium. Inset: fittings (—) of the absorbance values (●) at 467 nm.

## Appendix 2.

For a universe of 100 molecules the calculations were carried out as shown in the following example for 20% of total  $\mathbf{C}_t$  and 80% of total  $\mathbf{AH}^+$ , where the symbol

$$C_p^n = \frac{n!}{(n-p)!p!} \text{ represents the combination of } n \text{ elements } p \text{ to } p.$$

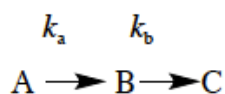
$$\mathbf{AH}^+ \cdot \mathbf{AH}^+ \quad C_2^{80} / C_2^{100}$$

$$\mathbf{AH}^+ \cdot \mathbf{C}_t (\mathbf{C}_t \cdot \mathbf{AH}^+) \quad C_1^{80} C_1^{20} / C_2^{100}$$

$$\mathbf{C}_t \cdot \mathbf{C}_t \quad C_2^{20} / C_2^{100}$$

Representation of the mole fraction distribution of the three bis-flavylium forms are shown below in **Figure A2(a)**.

Taking the trace of the flavylium disappearance to give *trans*-chalcone upon a direct pH jump from pH 1 to pH 5 reported in the inset of **Figure 8A**, it is easy to convert in the percentage of flavylium disappearance (and concomitant *trans*-chalcone formation), red lines in **Figure A2(b)**. At any time, we have the total percentage of conversion and thus the consequent fraction of  $\mathbf{AH}^+ \cdot \mathbf{AH}^+$ ,  $\mathbf{AH}^+ \cdot \mathbf{C}_t$ ,  $\mathbf{C}_t \cdot \mathbf{C}_t$ , black lines in **Figure A2(b)**. Fitting of the black lines can be carried out using a kinetic model



In this case  $k_a$  is two times the value of the first order rate constant of the global process  $k_{\text{obs}}$  in **Figure 8A**, and  $k_b$  is coincident with  $k_{\text{obs}}$ .

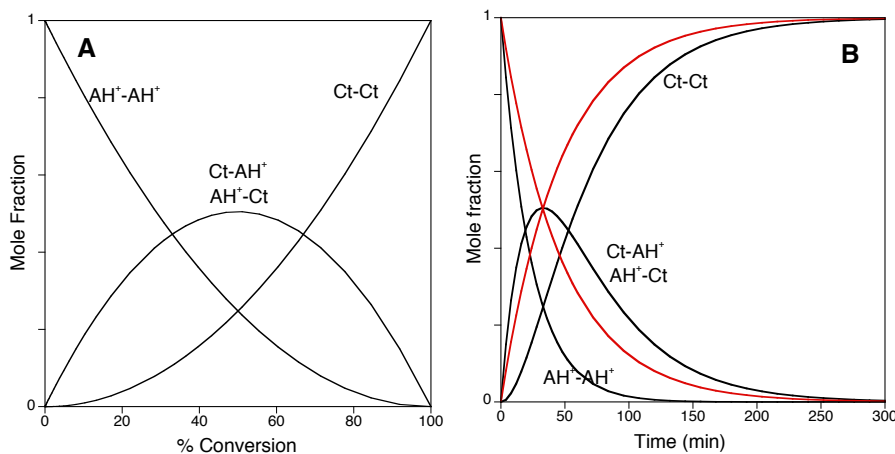


**Figure S2.** (A) Mole fraction distribution of the symmetric bis-flavylium compounds. (B) The same as a function of time. In red the observed kinetics of **Figure 8A**.

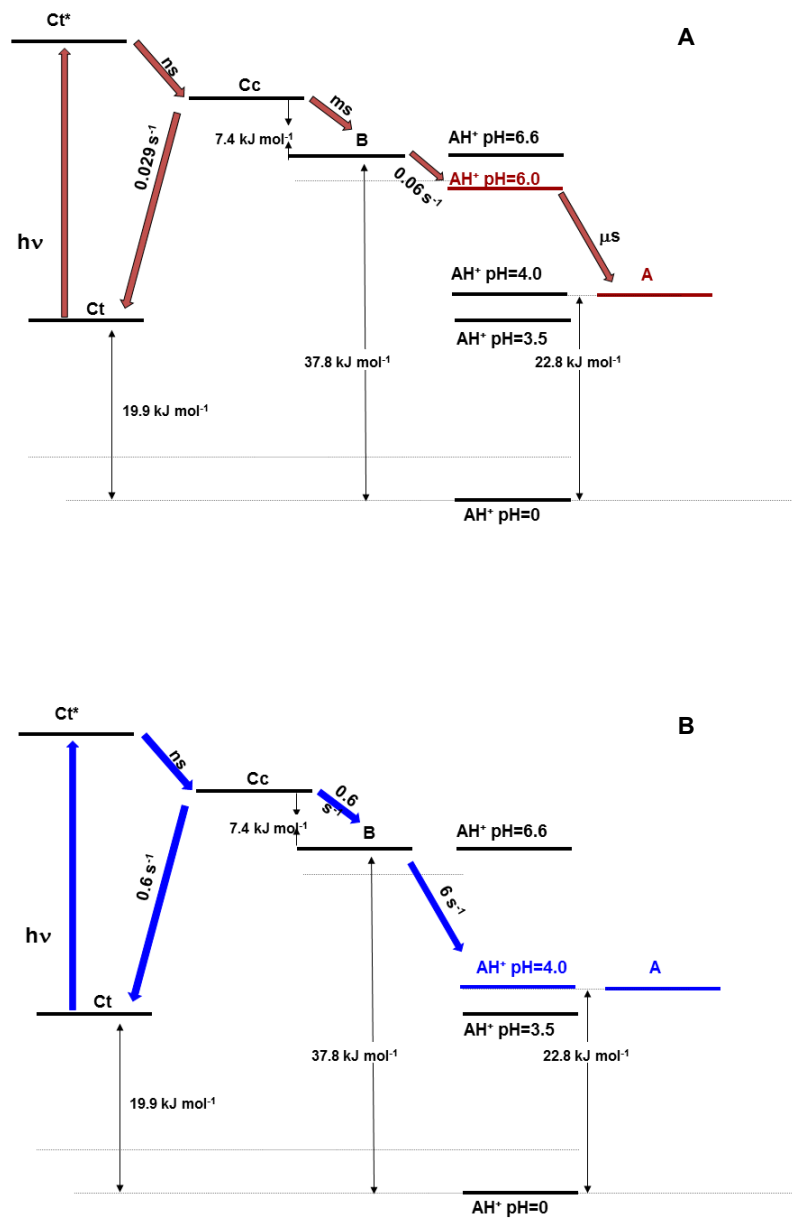
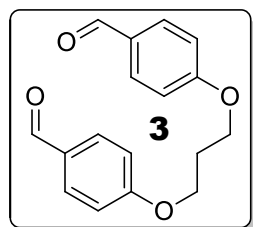
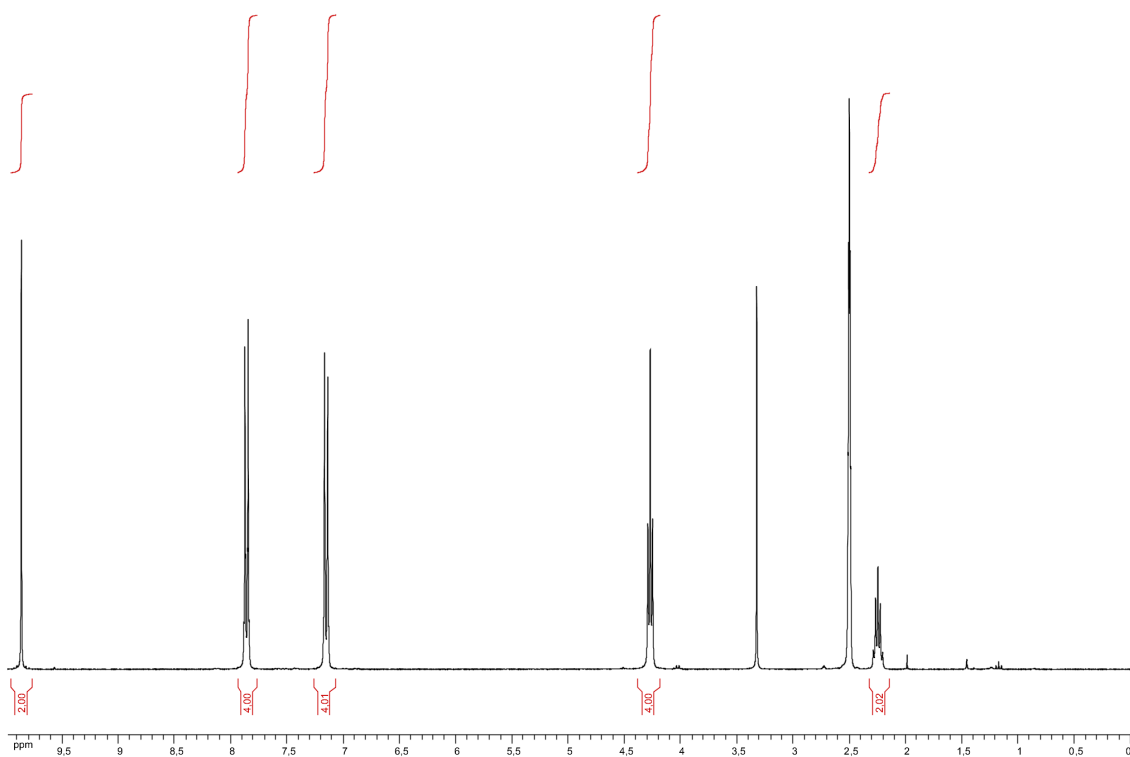


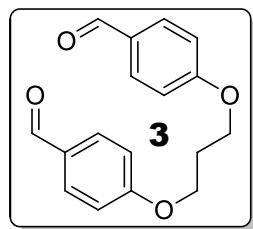
**Figure S3.** Energy-level diagram of bis-flavylium **2**. Illustration of the pathways upon irradiation of the trans-chalcone (**A**) at pH 6, where the rate-determining step is the hydration. (**B**) The same at pH 4 where the hydration is faster.

## Compilation of NMR spectra



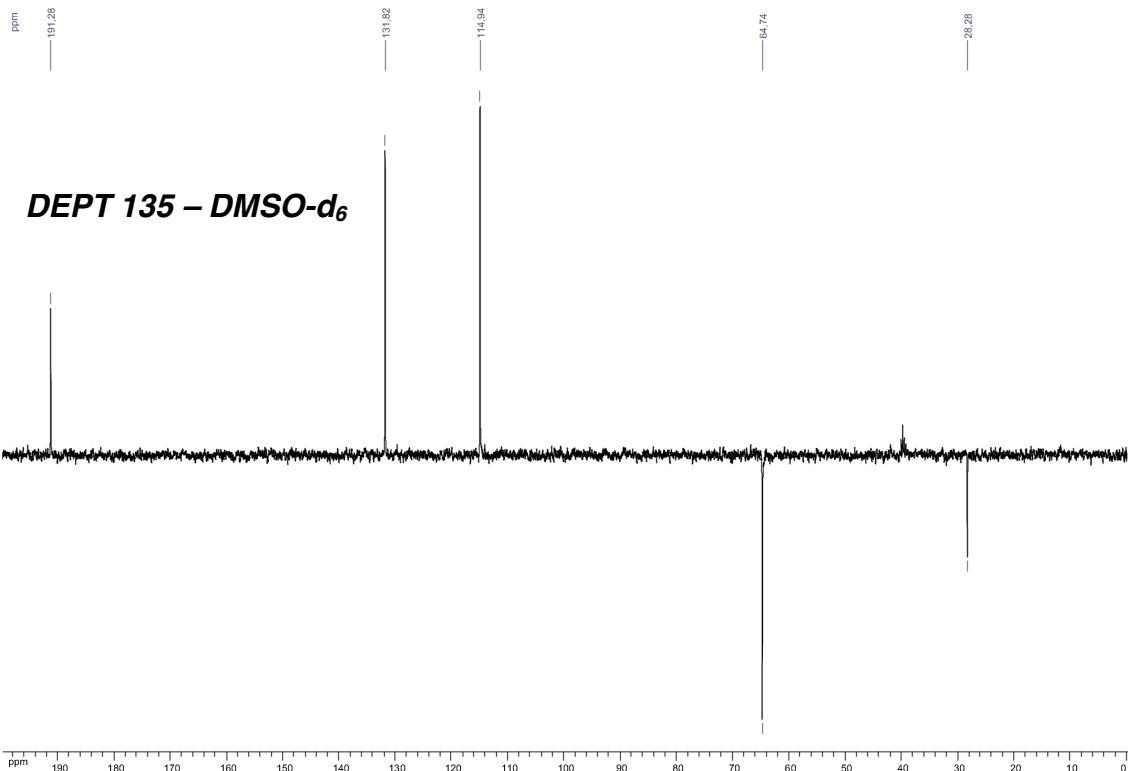
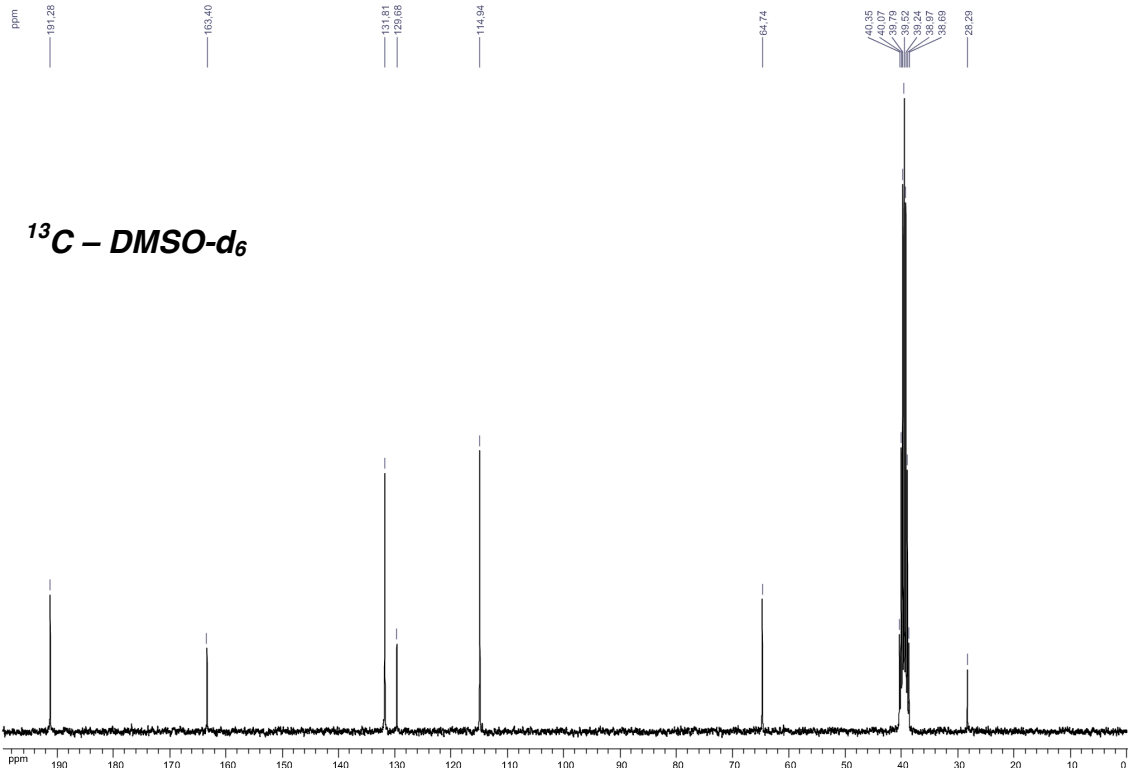
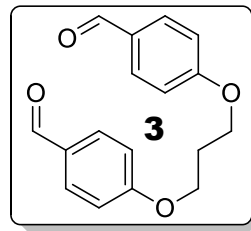
$^1H - DMSO-d_6$

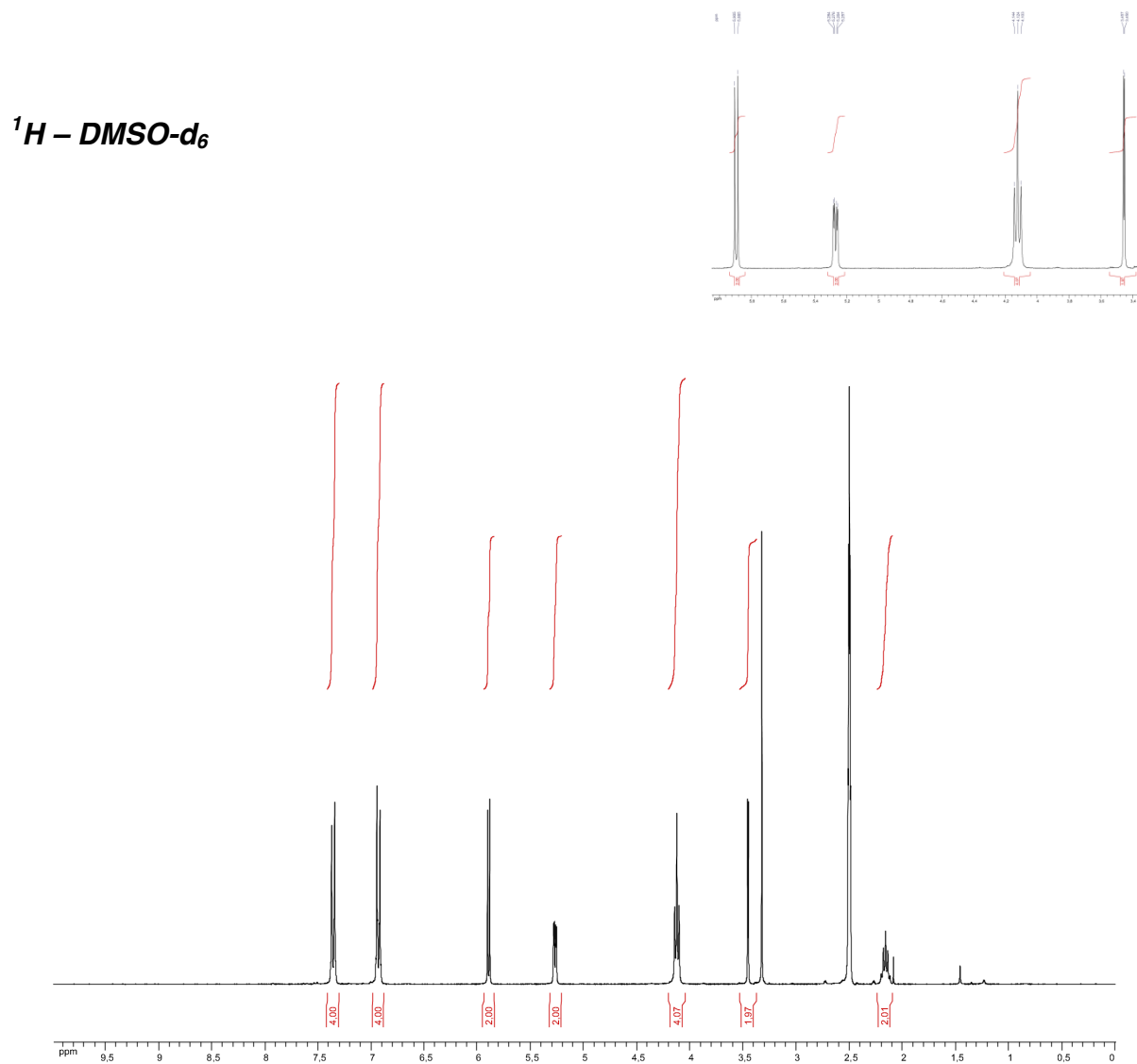
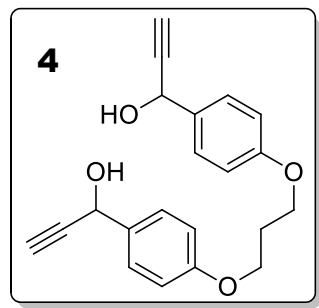


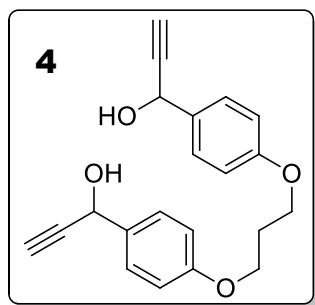


### *<sup>1</sup>H – DMSO-d<sub>6</sub> – LIST OF PEAKS*

Label	Intensity	Frequency(point)	Frequency(ppm)	Frequency(Hz)
1	197957312	20962	9,866	2961,567
2	148794288	27284	7,877	2364,614
3	161283488	27377	7,848	2355,832
4	145990112	29536	7,169	2151,97
5	134950992	29629	7,14	2143,188
6	67193752	38680	4,293	1288,551
7	147469760	38747	4,271	1282,224
8	69399616	38813	4,251	1275,992
9	100214008	44341	2,512	754,013
10	196914976	44359	2,506	752,313
11	263029808	44378	2,5	750,519
12	192957488	44398	2,494	748,631
13	93592520	44416	2,488	746,931
14	8887802	45055	2,287	686,594
15	32918756	45121	2,266	680,362
16	47281576	45186	2,246	674,224
17	30423476	45253	2,225	667,898
18	7831697	45319	2,204	661,666

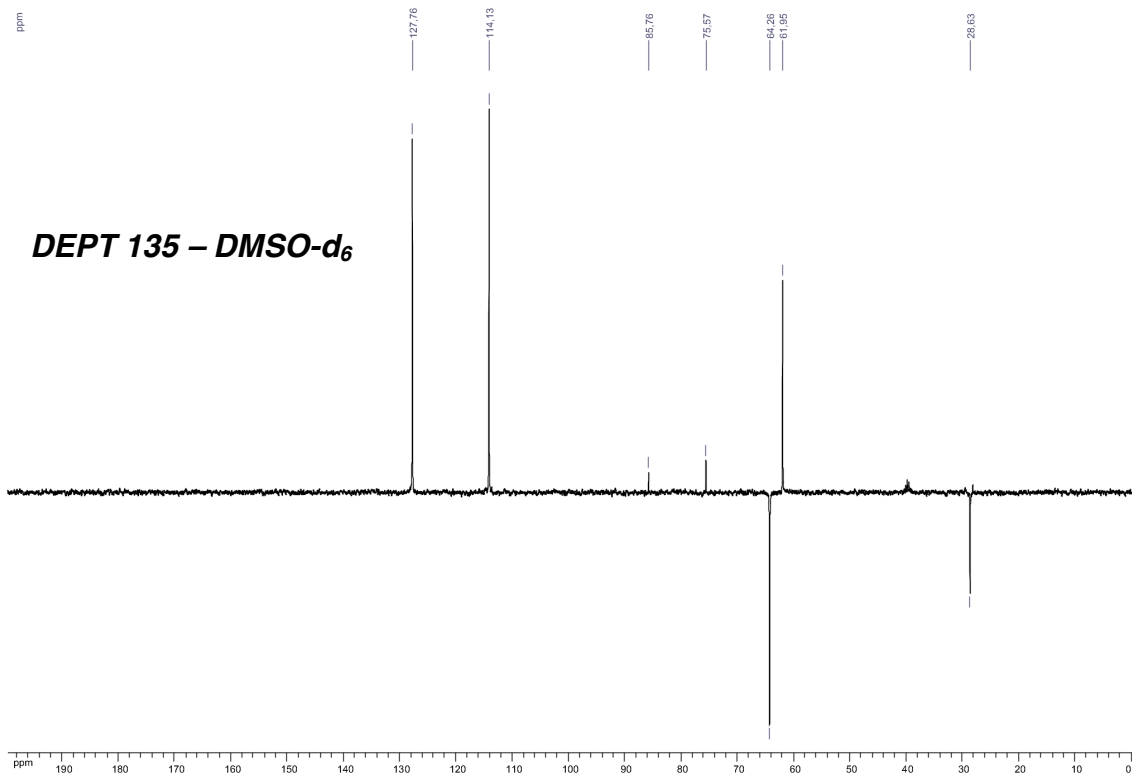
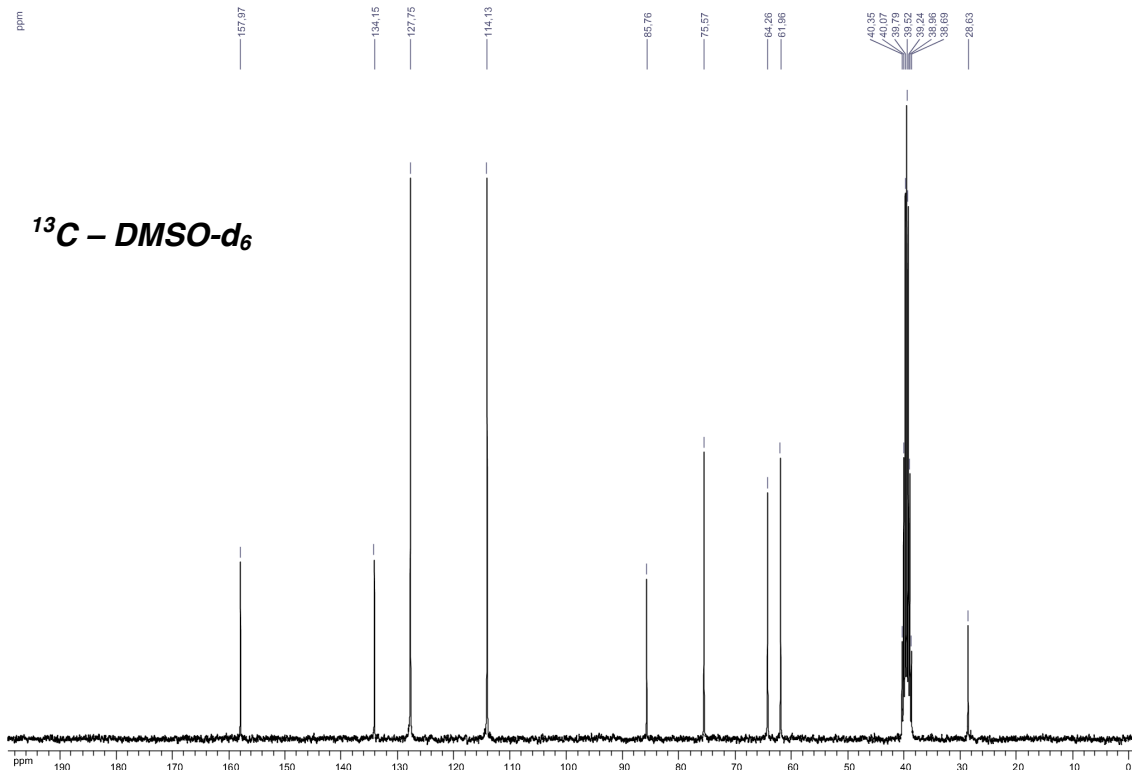
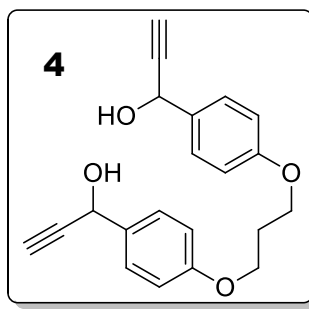


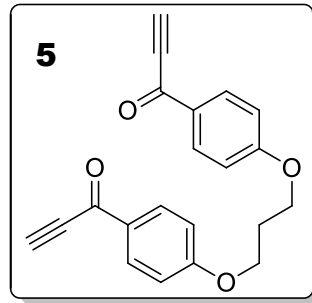




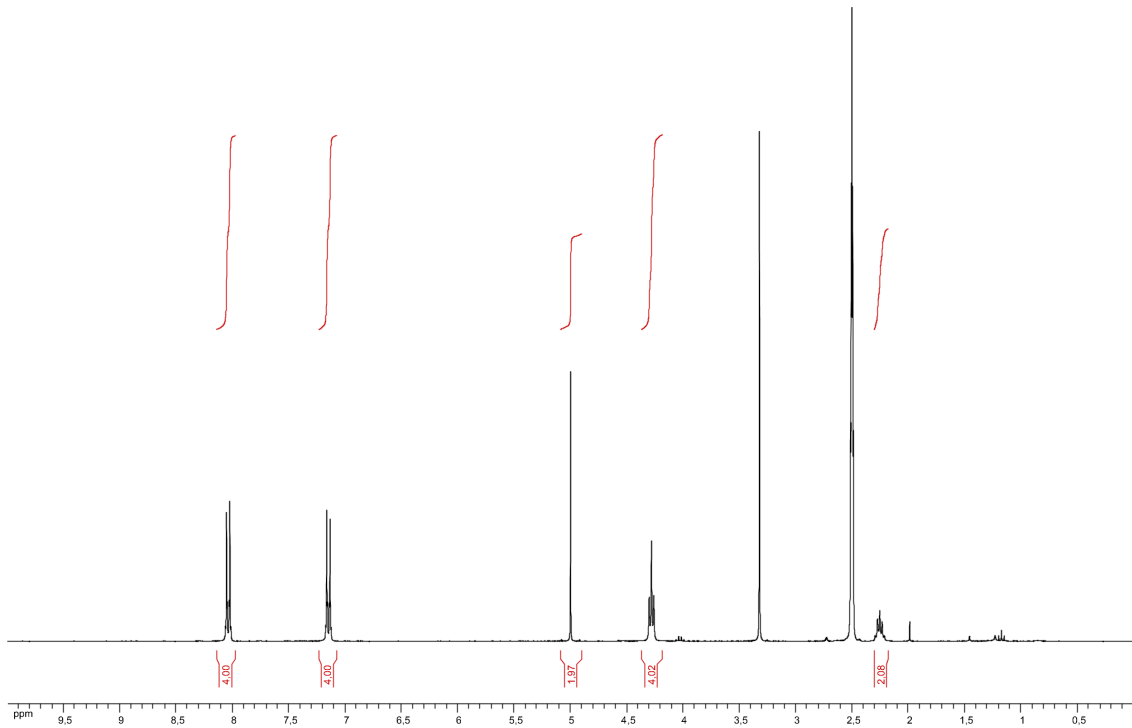
### *<sup>1</sup>H – DMSO-d<sub>6</sub>– LIST OF PEAKS*

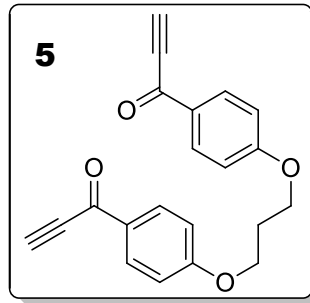
Label	Intensity	Frequency(point)	Frequency(ppm)	Frequency(Hz)
1	76929792	28889	7,373	2213,155
2	87992696	28980	7,344	2204,562
3	95912408	30242	6,947	2085,398
4	84317576	30335	6,918	2076,617
5	84221152	33555	5,905	1772,57
6	89549528	33618	5,885	1766,621
7	29500848	35530	5,284	1586,081
8	30272674	35553	5,276	1583,909
9	28706670	35592	5,264	1580,227
10	27728314	35615	5,257	1578,055
11	37483708	39152	4,144	1244,075
12	82640512	39218	4,124	1237,843
13	38080716	39284	4,103	1231,611
14	89655104	41336	3,457	1037,852
15	88280816	41359	3,45	1035,68
16	104344472	44341	2,512	754,105
17	212634784	44360	2,506	752,311
18	288750912	44379	2,5	750,517
19	207302112	44398	2,494	748,723
20	95948832	44417	2,488	746,929
21	5103983	45332	2,2	660,531
22	17544426	45397	2,18	654,393
23	25792292	45464	2,159	648,067
24	16377628	45530	2,138	641,835
25	4220612	45596	2,117	635,603





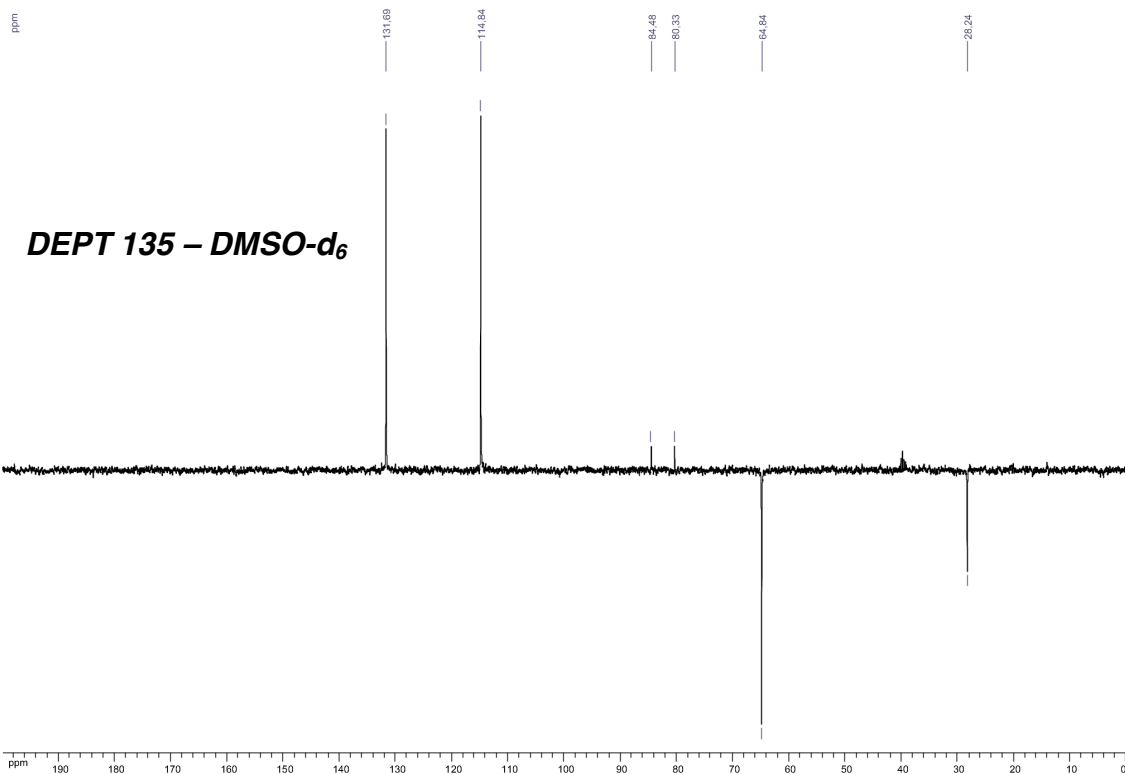
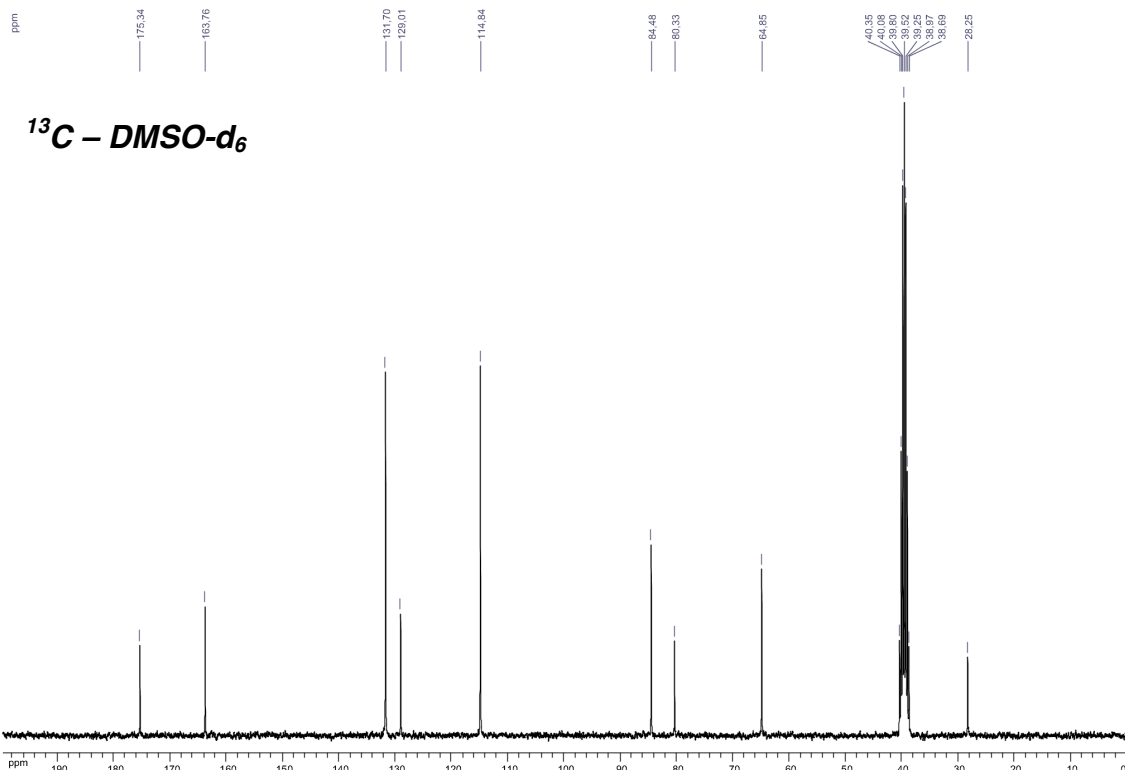
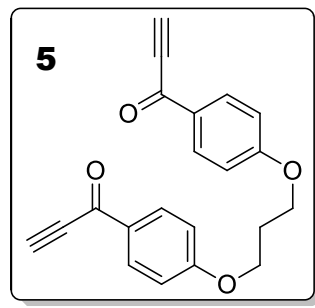
*<sup>1</sup>H – DMSO-d<sub>6</sub>*

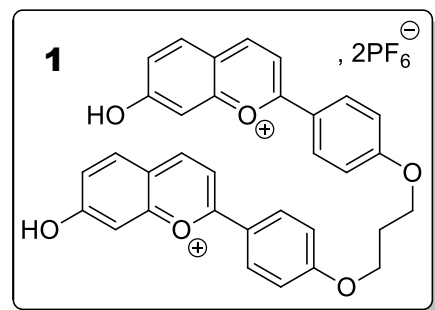




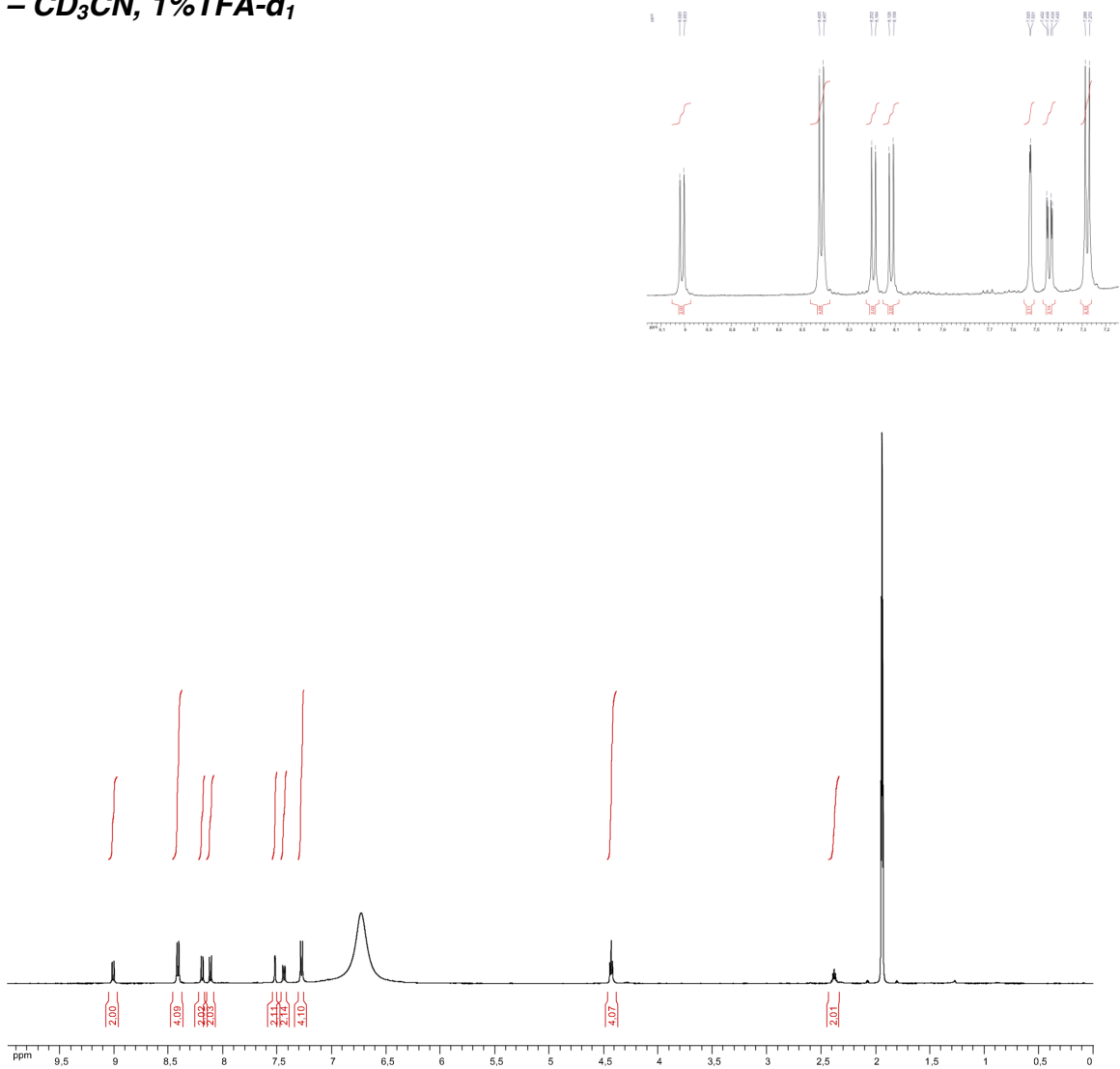
***<sup>1</sup>H – DMSO-d<sub>6</sub> – LIST OF PEAKS***

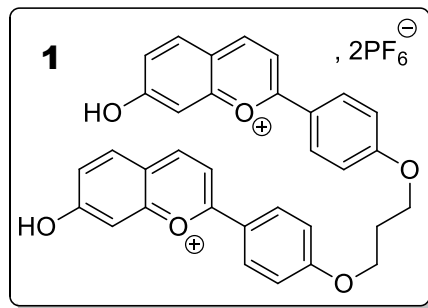
Label	Intensity	Frequency(point)	Frequency(ppm)	Frequency(Hz)
1	99042984	26723	8,054	2417,662
2	107724392	26818	8,024	2408,692
3	100639504	29553	7,164	2150,44
4	93845152	29648	7,134	2141,47
5	206767488	36436	4,999	1500,516
6	34047928	38654	4,301	1291,082
7	77094040	38720	4,28	1284,85
8	35276612	38786	4,259	1278,618
9	167798128	44341	2,512	754,089
10	351695840	44360	2,506	752,295
11	486154848	44379	2,5	750,501
12	349038176	44398	2,494	748,707
13	161631632	44418	2,488	746,818
14	4383196	45035	2,294	688,558
15	17368488	45099	2,274	682,515
16	23875100	45165	2,253	676,283
17	15288449	45231	2,232	670,051
18	4243509,5	45295	2,212	664,008





$^1\text{H} - \text{CD}_3\text{CN}, 1\% \text{TFA-}d_1$





**$^1\text{H} - \text{CD}_3\text{CN}, 1\% \text{TFA-}d_1 - \text{LIST OF PEAKS}$**

Label	Intensity	Frequency(point)	Frequency(ppm)	Frequency(Hz)
1	6186833	19499	9,02	4511,263
2	6482261	19556	9,003	4502,566
3	11754345	21451	8,425	4213,407
4	12231547	21510	8,407	4204,404
5	7940178,5	22183	8,202	4101,711
6	7693411	22240	8,184	4093,013
7	7615860,5	22431	8,126	4063,869
8	8110021	22490	8,108	4054,866
9	7705939,5	24401	7,525	3763,266
10	8065055	24413	7,521	3761,435
11	5259846	24640	7,452	3726,797
12	4763013	24654	7,448	3724,661
13	5128801,5	24698	7,434	3717,947
14	4685022	24713	7,43	3715,658
15	12246538	25177	7,288	3644,856
16	12184034	25236	7,27	3635,853
17	5975978,5	34501	4,443	2222,105
18	12406289	34541	4,431	2216,001
19	6421275	34581	4,419	2209,898
20	798485	41182	2,405	1202,649
21	2822890,75	41222	2,393	1196,546
22	4171530,25	41262	2,38	1190,442
23	2856909	41302	2,368	1184,339
24	875888,438	41342	2,356	1178,235

